

Postponing the dynamical transition density using competing interactions

Patrick Charbonneau · Joyjit Kundu

Received: date / Accepted: date

Abstract Systems of dense spheres interacting through very short-ranged attraction are known from theory, simulations and colloidal experiments to exhibit dynamical *reentrance*. The liquid state can thus be fluidized to higher densities than otherwise possible with interactions that are purely repulsive or long-ranged attractive. A recent mean-field, infinite-dimensional calculation predicts that the dynamical arrest of the fluid can be further delayed by adding a longer-ranged repulsive contribution to the short-ranged attraction. We examine this proposal by performing extensive numerical simulations in a three-dimensional system. We first find the short-ranged attraction parameters necessary to achieve the densest liquid state, and then explore the parameters space for an additional longer-ranged repulsion that could enhance the effect. In the family of systems studied, no significant (within numerical accuracy) delay of the dynamical arrest is observed beyond what is already achieved by the short-ranged attraction. Possible explanations are discussed.

1 Introduction

Particles with short-ranged attractive and long-ranged repulsive (SALR) interactions can form fairly elaborate structures [1–9]. Despite the spherical symmetry of their pair interaction potential, at low temperatures these models assemble into exotic ordered and disordered mesophases, and their structural richness has clear dynamical consequences, even

in the disordered regime [10–12]. A recent theoretical proposal suggests that certain SALR models exhibit unusual dynamical features in the very dense fluid regime [13] as well. Maimbourg *et al.* [13]’s extension of a high-dimensional treatment of the glass transition [14–16] suggests that certain models should display a very pronounced dynamical reentrance upon changing temperature. More precisely, the theoretical analysis suggests that a carefully chosen high-density SALR system that is glassy at low temperature should, upon heating, first melt and then get dynamically arrested once again, all while remaining completely disordered, i.e., without crystallizing.

On its own, such reentrance is not exceptional. The phase behavior of systems with core-softened interactions can exhibit multiple dynamically arrested phases leading to high-order singularities, as first proposed by mode-coupling theory [17–21], and then verified by both experiments [21–26] and numerical simulations [27–34]. Dynamical quantities, such as the density-density correlator, then exhibit a logarithmic decay instead of a typical two-step relaxation, and the mean-squared displacement grows sub-diffusively instead of plateauing at intermediate times. A common physical interpretation of this effect is that introducing short-ranged attraction leads to an interplay between two localization mechanisms: caging from the hard-core repulsion and interparticle bonding. As a result liquids with a higher packing fraction than is possible from either mechanism can then be stabilized [35]. Adding a supplementary, longer-ranged repulsion is understood as effectively deepening the well created by the short-range attraction, and thus leads to a slightly more efficient packing of neighboring spheres in the liquid state [13]. In the mean-field description, the nonergodicity transition to a glass phase is then pushed to even higher densities although only over a very narrow temperature window [13]. Even though this improvement over a system with purely short-ranged attraction is predicted to

Patrick Charbonneau
Department of Chemistry, Duke University, Durham, North Carolina
27708, USA
E-mail: patrick.charbonneau@duke.edu

Joyjit Kundu
Department of Physics, Duke University, Durham, North Carolina
27708, USA
E-mail: joyjitkundu032@gmail.com

be about 3% in the $d \rightarrow \infty$ limit, the effect should be large enough to be numerically distinguishable if it indeed persists in a finite-dimensional system. An additional methodological challenge, however, is that this transition is only a crossover away from the $d \rightarrow \infty$ limit [14].

In this article, we attempt to test this prediction in three dimensions via extensive numerical simulations. First, we tune the attraction range of a system of particles interacting via a hard core followed by a short-ranged square-well attraction (SW) to maximize the high-density extension of the liquid phase. We then optimize the interaction parameters of a system with an additional larger-ranged square-shoulder repulsion (SW+SS) in an attempt to push the dynamical arrest to even higher densities. The plan for the rest of this article is as follows. In Sec. 2 we describe the model, the simulation method and the observables of interest. In Sec. 3, we present the simulation results, and we briefly conclude in Sec. 4.

2 Models and Simulation Method

We study 50% – 50% binary (A-B) mixtures of $N = 1000$ spherical particles interacting via two potentials: (i) a simple square-well (SW) interaction, and (ii) a SALR square-well plus square-shoulder (SW+SS) interaction. The hard core diameter ratio of the two particle types, $\sigma_A/\sigma_B = 1.2$, with an additive hard-core interaction, i.e., $\sigma_{ij} = (\sigma_i + \sigma_j)/2 \forall ij$, is chosen so as to strongly suppress crystallization. The interaction potential can then be generically expressed as

$$V_{ij} = \begin{cases} \infty & r_{ij} \leq \sigma_{ij} \\ -U_0 & \sigma_{ij} < r_{ij} < \sigma_{ij} + \Delta_{ij}^0 \\ U_1 & \sigma_{ij} + \Delta_{ij}^0 < r_{ij} < \sigma_{ij} + \Delta_{ij}^0 + x \Delta_{ij}^1 \\ 0 & \sigma_{ij} + \Delta_{ij}^0 + x \Delta_{ij}^1 < r_{ij} \end{cases} \quad (1)$$

where $\Delta_{ij}^0 = \lambda_0 \sigma_{ij}$ and U_0 are the width and depth, respectively, of the square well, and $\Delta_{ij}^1 = \lambda_1 \sigma_{ij}$ and U_1 are the corresponding parameters for the square shoulder. Model (i) has $x = 0$, while model (ii) has $x = 1$, and in both cases temperature, T , is expressed in reduced units of U_0 with Boltzmann constant, k_B , set to unity. Hence, model (i) has a single tuning parameter, λ_0 , while model (ii) has three: λ_0 , λ_1 , and U_1 . We consider the dynamics of these systems at constant N , volume V and T using a Monte Carlo dynamics that only consists of N single-particle translations per unit time, t . These translations are taken along a vector randomly drawn within a three-dimensional cube of side $\delta\ell$, such that the relaxation time is minimum at a packing fraction close to the dynamical transition. The results of such Monte Carlo dynamics are known to be similar to those of other *local* dynamics in the dense fluid regime which is the regime of interest for this work [36–38].

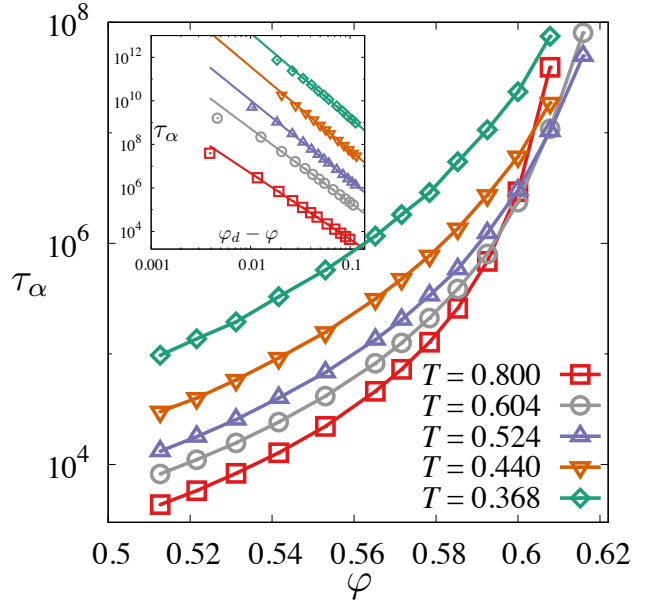


Fig. 1 The relaxation time τ_α as a function of the packing fraction ϕ for different temperatures. Inset: dynamical transition densities, $\phi_d(T)$, estimated by fitting the structural relaxation times to a power-law $\tau_\alpha(\phi; T) = A(\phi_d(T) - \phi)^{-\gamma}$. Results here are given for a model with $\lambda_0 = 0.019$, $\lambda_1 = 2.5$, $U_1 = 0.10$. Deviations from the power-law as $\phi \rightarrow \phi_d$ are due to activated cage escapes. For visual clarity, the vertical scale for $T = 0.800, 0.604, 0.524, 0.440$ and 0.368 has been multiplied by $10^0, 10^1, 10^2, 10^3$, and 10^4 , respectively.

Equilibration of the initial system is ensured by running Monte Carlo dynamics for at least ten structural relaxation times, τ_α , defined from the characteristic decay, $Q(\tau_\alpha) \equiv e^{-1}$, of the self-part of the particle-scale overlap function

$$Q(t) = \frac{1}{N} \sum_{i=0}^N \Theta(a - |r_i(t) - r_i(0)|), \quad (2)$$

where Θ is a step function and $a = 0.3\sigma_B$ is a microscopic length chosen to be close to the typical particle cage size. This function therefore represents the fraction of particles having moved a distance smaller than a by time t .

The equilibrium $Q(t)$ for the liquid is averaged over the trajectory that begins after equilibration. Typical plots for the relaxation time as a function of the packing fraction are shown in Fig. 1 for different temperatures. At fixed T , $\tau_\alpha(\phi; T)$ is used to estimate the (avoided) dynamical transition density, $\phi_d(T)$, by fitting to the critical scaling form, $\tau_\alpha(\phi; T) = A(\phi_d(T) - \phi)^{-\gamma}$ – see inset of Fig. 1. Because of the presence of activated processes in finite dimensions, this power-law scaling persists for at most a couple of decades [14], but this range suffices to provide a fairly robust estimate of ϕ_d . Estimation of $\phi_d(T)$ provides the dynamical diagram in the ϕ - T plane.

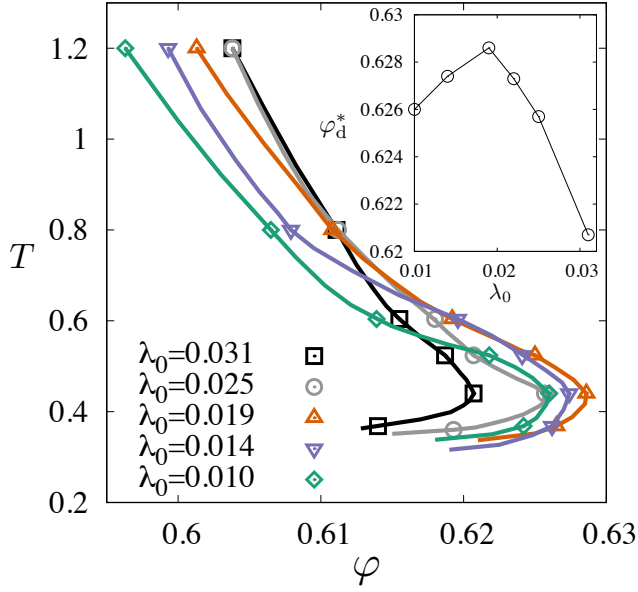


Fig. 2 Dynamical diagram for fluids of spheres interacting via a square-well attraction of different well widths λ_0 . Inset: the maximum fluid packing fraction φ_d^* accessible from the liquid side for different ranges of attraction λ_0 .

3 Results and Discussion

We first tune the interaction range of the simple SW system in order to maximize the depth of the fluid pocket. To the best of our knowledge this optimization had not been previously attempted in simulations. Most previous studies considered models with $\lambda_0 = 0.03$, following the MCT prediction for the existence of an anomalous glassy regime for that interaction range. The dynamical diagrams for different λ_0 around 3% are shown in Fig. 2; the dynamical reentrance of the liquid is clearly visible. The maximum accessible liquid density, φ_d^* , is however, not attained with $\lambda_0 = 0.03$, but rather with one of $\lambda_0^* \approx 0.019$. Although our result for $\lambda_0^* \approx 0.019$ is in the vicinity of the infinite-dimensional theoretical prediction for this optimization ($\lambda_0^* \approx 0.029$) [13], it is nonetheless significantly different from it. Because the intricate liquid structure of finite-dimensional systems is neglected in the analytical study, this discrepancy is not particularly surprising. In three dimensions, the nearest-neighbor shell structure is indeed much tighter than what is theoretically assumed. A possible explanation for the discrepancy is therefore that a smaller attraction range suffices in simulations to obtain an energetic stabilization comparable to what is expected in the $d \rightarrow \infty$ limit.

We next explore whether adding a suitably tuned repulsive part to the potential can further delay the dynamical arrest. In this case, three parameters are to be optimized: λ_0 , λ_1 , and U_1 . We expect the three-dimensional parameter space ($\lambda_0, \lambda_1, U_1$) for the SW+SS system to be simple

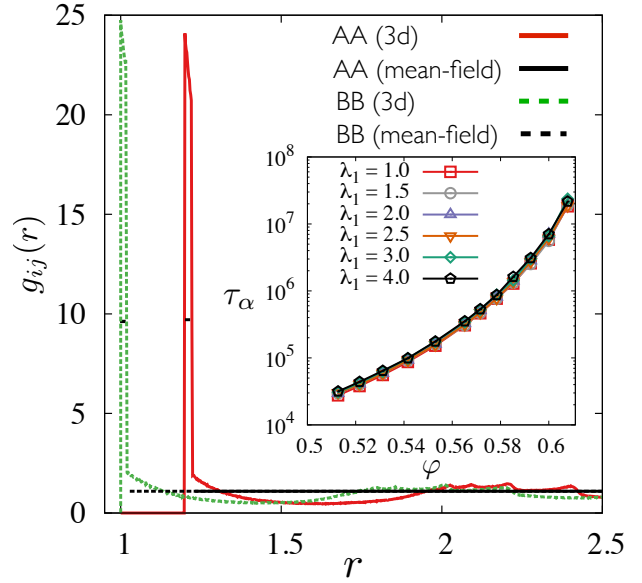


Fig. 3 Partial pair correlation function $g_{ij}(r)$ for A and B particles. The liquid shell structure is much stronger in $d = 3$ than in the $d \rightarrow \infty$ limit. Inset: the evolution of τ_α with φ is remarkably insensitive to the choice of λ_1 , but very small deviations can be seen when $\lambda_1 > 2.5$.

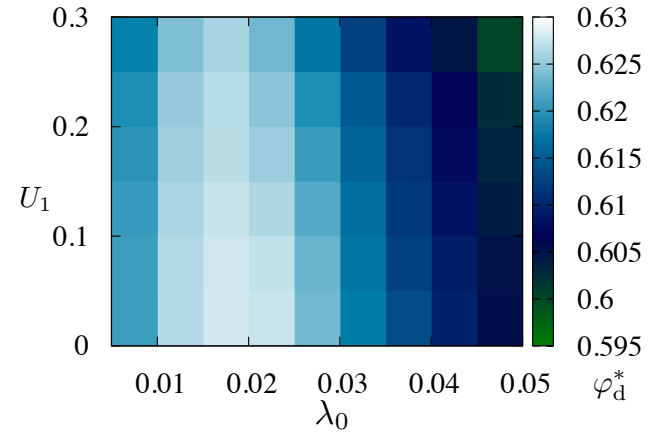


Fig. 4 Maximal fluid packing fraction φ_d^* for the SW+SS system in the parameter space of U_1 and λ_0 for $\lambda_1 = 2.5$. The line $U_1 = 0$ corresponds to the SW system. This plot reveals that longer-ranged repulsion does not significantly push φ_d^* to higher densities in three dimensions, but nonetheless gives rise to a parameter pocket of enhanced reentrance around $\lambda_0 \approx 0.019$, away from the $U_1 = 0$ axis.

with a single minimum (corresponding to the densest liquid configuration) connected to the minimum of the SW system ($U_1 = 0, \lambda_1 = 0$) through a path without large barriers. To nonetheless ensure that our optimization does not miss its target, we explore a wide range of parameter values. We search for an optimum over $\lambda_0 \in (0.010, 0.060)$, $\lambda_1 \in (0.5, 5.0)$, and $U_1 \in (0.0, 0.40)$ by gridding the parameter space, and compute φ_d for a few temperatures around the reentrance regime in the dynamical diagram for each grid point to estimate φ_d^* . From this scheme we identified the set

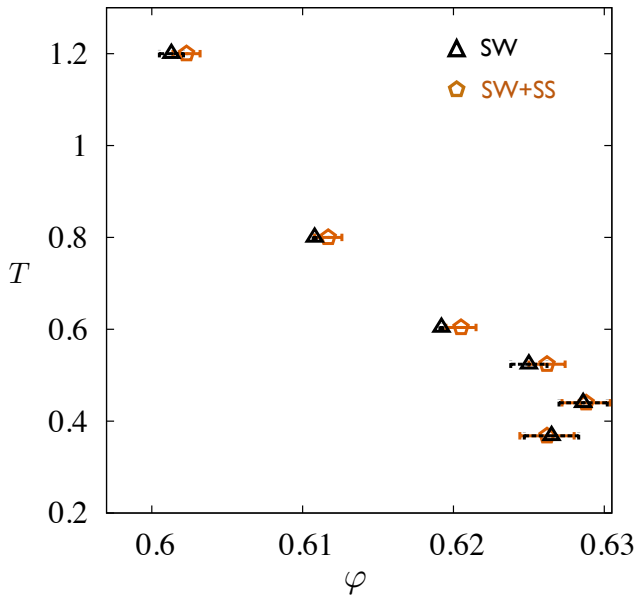


Fig. 5 Dynamical diagram for the SW system with $\lambda_0 = 0.019$ and the SW+SS system with optimized parameters ($\lambda_0 = 0.019$, $\lambda_1 = 2.5$, $U_1 = 0.10$). Adding longer-ranged repulsion does not significantly push ϕ_d^* to higher densities in these models.

of parameters that pushes the dynamical transition furthest as $\lambda_0^* = 0.019 \pm 0.004$, $U_1^* \leq 0.10$, and $0.8 \leq \lambda_1^* \leq 3.0$. All directions away from this optimum lead to lower or comparable values of ϕ_d^* . The optimal parameters identified are in qualitative agreement with the theoretical prediction that the repulsion should be much weaker and longer ranged than the attraction and that the attraction range does not markedly broaden in going from a SW to a SW+SS model. In our case, however, the attraction range barely changes, while the theoretical prediction has λ_0^* increase from $0.029 \rightarrow 0.054$. Here again, the tightness of the finite-dimensional neighbor shell is likely at play.

A more significant difference is that while the dynamics (and thus ϕ_d) is somewhat sensitive to the repulsion strength U_1 , its dependence on the repulsion range λ_1 is much weaker over the parameter window considered. The dynamics of all models with $\lambda_1 \in [0.5, 2.5]$ indeed roughly coincides (see Fig. 3 inset). Once more, the pronounced shell structure of three-dimensional dense fluid is likely at play. While in the $d \rightarrow \infty$ limit, $g(r) = \exp(-\beta V_{ij}(r))$, and hence self-solvation can be strongly impacted by the interaction potential; in three dimensions, the influence of the hard core-repulsion is felt much more strongly (see Fig. 3). As a result, adding a weak repulsive contribution to the interaction potential results in a much weaker dynamical effect. For a repulsion range that falls within the intershell depletion regime, no notable effect on the dynamics are thus observed.

Given the relative insensitivity of the optimization to λ_1 , we can concentrate on the two-dimensional parameter space,

$\lambda_0 - U_1$, for ϕ_d^* . Fig. 4 shows the maximum fluid packing fraction ϕ_d^* in the space of U_0 and λ_1 where $\lambda_1 = 2.5$. Interestingly, the optimization landscape is relatively flat along U_1 . The SW optimum is therefore connected by a fairly soft mode to the SW+SS optimum. Along λ_1 , by contrast, ϕ_d^* changes much more rapidly. This landscape projection is therefore consistent with the above discussion.

The resulting dynamical diagrams for the SW and the SW+SS optima are compared in Fig. 5. The results show that the corresponding $\phi_d(T)$ values are not significantly different (within numerical uncertainty) from one another. If any enhancement of the reentrance pocket is present, it is therefore much smaller than the 3%, predicted by the $d = \infty$ calculation.

4 Conclusion

Motivated by a recent mean-field prediction that the dynamically sluggish fluid regime for models with SALR interactions can be pushed to higher densities than for models with purely short-ranged attraction, we have performed extensive Monte Carlo simulations of a family of SW and SW+SS models. Our exploration of model parameters did not identify (within numerical uncertainty) any SALR model that pushes the dynamical transition significantly beyond the densest packing achievable by only short-ranged attraction. We did, however, identify a branch of parameters over which the optimum extends. This nontrivial feature could be a finite dimensional echo of the $d \rightarrow \infty$ prediction. The theoretical prediction that further tuning the interaction potential could engender additional (smaller) gains in ϕ_d^* [13] is nevertheless unlikely to be verifiable in three-dimensional systems.

Data associated with this work are available from the Duke Digital Repository at “will be added”.

Acknowledgements This paper is dedicated to the late Bob Behringer, who has always been warm, wise and supportive to this junior colleague (PC). He will be sorely missed. We acknowledge funding from the Simons Foundation (Grant # 454937 to PC) and computer time of Duke Compute Cluster (DCC) and Extreme Science and Engineering Discovery Environment (XSEDE), supported by National Science Foundation grant number ACI-1548562.

References

1. A. Stradner, H. Sedgwick, F. Cardinaux, W. C. K. Poon, S. U. Egelhaaf, and P. Schurtenberger, *Nature* **432**, 492 (2004).
2. E. Mani, W. Lechner, W. K. Kegeld, and P. G. Bolhuis, *Soft Matter* **10**, 4479 (2014).
3. Y. Zhuang and P. Charbonneau, *J. Phys. Chem. B* **120**, 6178 (2016).

4. A. Ciach, J. Pekalski, and W. T. Gozdz, *Soft Matter* **9**, 6301 (2013).
5. B. A. Lindquist, R. B. Jadrich, D. J. Milliron, and T. M. Truskett, *J. Chem. Phys.* **145**, 074906 (2016).
6. J. A. Bollinger and T. M. Truskett, *J. Chem. Phys.* **145**, 064902 (2016).
7. J. A. Bollinger and T. M. Truskett, *J. Chem. Phys.* **145**, 064903 (2016).
8. R. B. Jadrich, B. A. Lindquist, and T. M. Truskett, *J. Chem. Phys.* **146**, 184103 (2017).
9. C. Cao, X. Huang, C. B. Roth, and E. R. Weeks, *The Journal of Chemical Physics* **147**, 224505 (2017).
10. Y. Zhuang and P. Charbonneau, *J. Chem. Phys.* **147**, 091102 (2017).
11. A. Coniglio, L. D. Arcangelis, E. D. Gado, A. Fierro, and N. Sator, *J. Phys.: Condens. Matter* **16**, S4831 (2004).
12. T. Abete, A. de Candia, E. D. Gado, A. Fierro, and A. Coniglio, *Phys. Rev. Lett.* **98**, 088301 (2007).
13. T. Maimbourg, M. Sellitto, G. Semerjian, and F. Zamponi, *SciPost Phys.* **4**, 039 (2018).
14. P. Charbonneau, J. Kurchan, G. Parisi, P. Urbani, and F. Zamponi, *Annu. Rev. Condens. Matter Phys.* **8**, 265 (2017).
15. M. Sellitto and F. Zamponi, *J. Phys.: Conf. Ser.* **473**, 012020 (2013).
16. M. Sellitto and F. Zamponi, *Eur. Phys. Lett.* **103**, 46005 (2013).
17. L. Fabbian, W. Götze, F. Sciortino, P. Tartaglia, and F. Thiery, *Phys. Rev. E* **59**, R1347 (1999).
18. J. Bergenholtz and M. Fuchs, *Phys. Rev. E* **59**, 5706 (1999).
19. K. Dawson, G. Foffi, M. Fuchs, W. Götze, F. Sciortino, M. Sperl, P. Tartaglia, T. Voigtmann, and E. Zaccarelli, *Phys. Rev. E* **63**, 011401 (2000).
20. W. Götze and M. Sperl, *Phys. Rev. E* **66**, 011405 (2002).
21. X. qiang Chu, M. Lagi, E. Mamontov, E. Fratini, P. Baglioni, and S.-H. Chen, *Soft Mater.* **6**, 2623 (2010).
22. K. N. Pham, A. M. Puertas, J. Bergenholtz, S. U. Egelhaaf, A. Moussaïd, P. N. Pusey, A. B. Schofield, M. E. Cates, M. Fuchs, and W. C. K. Poon, *Science* **296**, 104 (2002).
23. S.-H. Chen, W.-R. Chen, and F. Mallamace, *Science* **300**, 619 (2003).
24. T. Eckert and E. Bartsch, *Phys. Rev. Lett.* **89**, 125701 (2002).
25. F. Mallamace, P. Gambadauro, N. Micali, P. Tartaglia, C. Liao, and S.-H. Chen, *Phys. Rev. Lett.* **84**, 5431 (2000).
26. X. Lu, S. G. J. Mochrie, S. Narayanan, A. R. Sandy, and M. Sprung, *Phys. Rev. Lett.* **100**, 045701 (2008).
27. N. Gnan, G. Das, M. Sperl, F. Sciortino, and E. Zaccarelli, *Phys. Rev. Lett.* **113**, 258302 (2014).
28. F. Sciortino, P. Tartaglia, and E. Zaccarelli, *Phys. Rev. Lett.* **91**, 268301 (2003).
29. E. Zaccarelli, G. Foffi, K. A. Dawson, S. V. Buldyrev, F. Sciortino, and P. Tartaglia, *Phys. Rev. E* **66**, 041402 (2002).
30. A. J. Moreno and J. Colmenero, *J. Chem. Phys.* **124**, 184906 (2006).
31. A. J. Moreno and J. Colmenero, *J. Phys.: Condens. Matter* **19**, 466112 (2007).
32. G. Foffi, K. A. Dawson, S. V. Buldyrev, F. Sciortino, E. Zaccarelli, and P. Tartaglia, *Phys. Rev. E* **65**, 050802(R) (2002).
33. A. M. Puertas, M. Fuchs, and M. E. Cates, *Phys. Rev. Lett.* **88**, 098301 (2002).
34. P. Charbonneau and D. R. Reichman, *Phys. Rev. Lett.* **99**, 135701 (2007).
35. F. Sciortino, *Nat. Mater.* **1**, 145 (2002).
36. L. Berthier, *Phys. Rev. E* **76**, 011507 (2007).
37. L. Berthier and W. Kob, *J. Phys.: Condens. Matter* **19**, 205130 (2007).
38. G. Rutkai and T. Kristóf, *J. Chem. Phys.* **132**, 104107 (2010).